Coadsorption phase diagram for CH_4/CCl_4 on graphite

William J. Weber* and David L. Goodstein
Condensed Matter Physics 114-36, California Institute of Technology, Pasadena, California 91125, USA
(Received 17 January 2006; published 30 May 2006)

We present an extensive thermodynamic study of methane coadsorbed on graphite precoated with a saturated monolayer of carbon tetrachloride. A combination of heat capacity and volumetric equation of state data permit construction of the multilayer coadsorption phase diagram between 70 and 115 K. Displacement of the preadsorbed CCl_4 by CH_4 occurs by a continuous process across the temperature range studied. While the continuous nature of the transition implies a single phase mixed film during displacement, the observation of a commensurability transition characteristic of CH_4 on bare graphite suggests the emergence of order in the coadsorbed CH_4 in the early stages of displacement. At low temperatures and multilayer coverages, the coadsorption phase diagram shows small but measurable differences from the pure CH_4 data, indicating that the multilayer film formed after displacement is not identical to that of CH_4 in the absence of CCl_4. At higher temperatures, a new first order phase transition is observed to correspond with the completion of displacement. One interpretation is that the phase boundary represents the melting of a nearly pure CH_4 monolayer solid into a mixed liquid film phase, with the size of the melting point depression indicating a concentration of nearly 1% CCl_4 in the liquid phase.

DOI: 10.1103/PhysRevB.73.195424 PACS number(s): 68.43.−h, 68.35.Rh, 64.75.+g, 64.30.+t

I. INTRODUCTION

Simultaneous coadsorption of two distinct chemical species on an atomically smooth substrate such as exfoliated graphite is an ideal system for studying a host of interesting condensed matter phenomena, including phase transitions, miscibility, and competition between different forms of order, all coupled with the evolution from two- to three-dimensional behavior as the film thickens. One interesting class of coadsorption system, typically studied at liquid nitrogen temperatures, involves a preadsorbed monolayer of a highly condensable, low vapor pressure material (such as CCl_4, SF_6, or C_6H_{12}) followed by introduction of a relatively inert gas species (such as Kr, CH_4, or Xe).[1–12] These systems exhibit displacement, in which the more strongly binding preadsorbate film is displaced off the graphite surface by the more weakly interacting gas species. This novel phenomenon has been explained[4,11] by the incomplete-wetting nature of the preadsorbed film, which is unstable towards the nucleation of bulk crystals in the presence of a film of the more inert species. Techniques for investigating such systems have included: volumetric isotherm measurements of the equation of state, which exploit the measurable vapor pressure of the more volatile species; calorimetry measurements, which can detect phase transitions and desorption; and x-ray and neutron diffraction studies, which directly probe the structural order of the film.

This paper presents a detailed calorimetric-volumetric study of CH_4 on graphite that has been precoated with a saturated monolayer of CCl_4 between 70 and 115 K. This system was first studied by Dupont-Pavlovsky *et al.*[7] who observed displaclement of CCl_4 by CH_4 at 77 K to occur by a continuous process, with the CH_4 component reaching monolayer density continuously, adsorbing over a range of vapor pressures. This implies, by the Gibbs phase rule, a single phase mixed film in which the CH_4 concentration continuously increases to displace CCl_4 without ever nucleating a separate phase. This was in contrast with other systems, such as Kr/CCl_4 (Ref. 5) and Kr/C_6H_{12},[7] which, at 77 K, exhibit a discontinuous jump in the number of atoms adsorbed at a single vapor pressure, observed as a vertical step in the coadsorption isotherm, characteristic of a first-order displacement transition, in which a Kr domain separates from, and grows at the expense of, the preadsorbate film. The observation of continuous displacement was confirmed and extended to temperatures in excess of 100 K by another volumetric study.[11] This also showed, at the higher temperatures of the study, displacement becoming a multilayer phenomenon, with the coadsorbed CH_4 film density not approaching that of pure CH_4 on graphite until film coverages of nearly two layers.

The study of Dupont-Pavlovsky *et al.* also included neutron diffraction structural measurements, which gave a surprising and apparently contradictory result. The measurements showed, with increasing CH_4 coverage, a decrease in the amplitude of the two-dimensional (2D) CCl_4 solid Bragg reflection peak, accompanied by the growth of a peak corresponding to the 3D CCl_4 solid lattice constant, consistent with the picture of displacement of the CCl_4 film into the bulk crystal phase. However, also observed was a Bragg reflection peak indicating a distinct CH_4 solid film phase coexisting with the CCl_4 film, over a range of coverages. Phase separation of distinct 2D CH_4 and CCl_4 domains is inconsistent with the volumetric isotherm data, which showed displacement occurring over a range of vapor pressure, indicating displacement by a continuous, single phase process. Two phase film coexistence, over a range of vapor pressure and in equilibrium with the bulk solid CCl_4, would violate the Gibbs phase rule. This surprising result helped motivate this investigation of the CH_4/CCl_4 coadsorption system in our calorimeter, which is well suited to studying the phases of the coadsorbed film over a wide range of temperature.

We recently published a similar calorimetric and volumetric study of Kr/CCl_4 coadsorbed on graphite between 77 and 130 K.[12] The study showed displacement to be a continuous

transition for higher temperatures, with a suggested displacement critical temperature slightly below 90 K (the displacement transition had been observed to be first order at 77 K, by both volumetric and x-ray diffraction measurements).[5] A desorption heat capacity signal was observed to accompany the observed evaporation of the Kr monolayer as the system moved to higher temperatures and lower Kr coverages, indicating CCl_4 reversibly reclaiming the graphite surface as displacement is undone. At higher coverages and lower temperatures, the heat capacity features corresponding to phase transitions in the second, third, and fourth film layers of Kr were observed to fall on the same phase boundaries, in $(T, \delta\mu_{Kr})$, as previously measured for Kr on bare graphite without CCl_4, indicating that displacement runs to completion, resulting in a pure film of Kr on graphite. At temperatures above 112 K, however, the system displays a new first-order phase transition that is not present for Kr single-species adsorption on graphite and that coincides with the completion of displacement at these high temperatures. While the nature of the phase transition is not clear, a possible explanation could be Kr first layer melting, occurring at a depressed melting point due to CCl_4 impurities in the liquid phase. Investigation of this hypothesis is difficult with our calorimeter, as the pure Kr first layer melting curve exits the useful range of the apparatus (roughly 130 K) for coverages just above 1 monolayer.

The CH_4/CCl_4 coadsorption system offers better possibilities for investigating the fate of the CH_4 monolayer formed during displacement. The monolayer film for pure CH_4 on graphite features commensurate, dense, and expanded solid phases, in addition to a liquid phase (see Ref. 13 and the pure CH_4 data in Fig. 2). The relevant phase boundaries for 1-2 layer coverages fall in the range 95–105 K, and thus at temperatures and pressures easily accessible to our apparatus. Whether or not these phase boundaries exist in the coadsorption system and, if so, how and where in the $(T, \delta\mu_{CH_4})$ plane, is a sensitive probe of the state of the film that is formed by displacement of the CCl_4 monolayer. We know, from the volumetric isotherm measurements, that CH_4 displaces CCl_4 in continuous fashion, resulting in a film with an equation of state very similar to CH_4 on bare graphite. Investigating the phase boundaries with sensitive calorimetry measurements not only probes the state of the post-displacement "CH_4" film, but also addresses the interesting question of how the coadsorption system passes from a solid CCl_4 monolayer into a multilayer CH_4 film.

II. OVERVIEW OF THE CH_4/CCl_4 COADSORPTION PHASE DIAGRAM

To orient the reader for the lengthy experimental discussion that follows, we begin here by summarizing the conclusions for the CH_4/CCl_4 coadsorption phase diagram. The proposed phase diagram, plotted in $(T, |\delta\mu_{CH_4}|^{-1/3})$ in the plane of bulk solid saturation for CCl_4 ($\delta\mu_{CCl_4}=0$) is shown in Fig. 1. Here, $\delta\mu_{CH_4}(\equiv\mu_{CH_4}-\mu^0_{CH_4})$ is the chemical potential measured with respect to the bulk saturated CH_4 chemical potential, $\mu^0_{CH_4}(T)$. The rough proportionality of

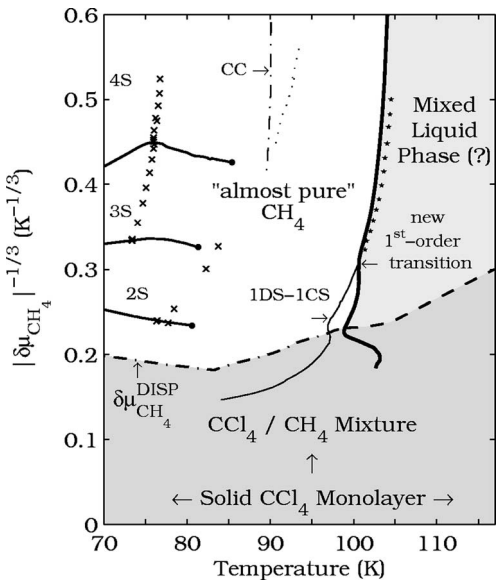

FIG. 1. Proposed phase diagram for CH_4 on graphite coated with a saturated monolayer of CCl_4.

$|\delta\mu_{CH_4}|^{-1/3}$ to film thickness in typical adsorption systems[14–16] makes it the natural choice for expressing multilayer phase diagrams, giving approximately equal spacing between different layers. For displaying smaller portions of the phase diagram, we use $\delta\mu_{CH_4}$.

At $|\delta\mu_{CH_4}|^{-1/3}=0$ in the coadsorption system, we start with a saturated monolayer of pure CCl_4. As CH_4 is introduced, it adsorbes continuously into the CCl_4 film to form a mixture that becomes richer in CH_4 as CCl_4 is displaced with increasing chemical potential. Below 100 K, displacement becomes very nearly complete upon crossing the line, $\delta\mu^{disp}_{CH_4}(T)$ (marked "-·-" in Fig. 1), where the film density of CH_4 in the coadsorption system becomes equal to that of pure CH_4 on graphite, within the resolution of our coverage measurements. Though this is a continuous transition at all temperatures studied, an observed sharp onset of CH_4 desorption upon entering the lower $|\delta\mu_{CH_4}|^{-1/3}$ mixed film regime suggests a true phase boundary.

While the CH_4 film densities in the pure and coadsorbed films become equal at $\delta\mu^{disp}_{CH_4}(T)$, calorimetry data reveal significant differences in the upper layer phase diagrams. Layer triple points are observed, but at measureably different temperatures, and, additionally, melting in the higher layers (marked with "×" in Fig. 1) appears to occur as a single phase transition, not as the crossing of two nearby phase boundaries as seen for single species CH_4 adsorption. The "CH_4 multilayer" formed by displacement in the coadsorption system is thus not simply pure CH_4 on graphite. This stands in contrast to the Kr/CCl_4 system, where we found second and third layer phase diagrams identical to those of pure Kr adsorbed on graphite.

In the white region of the "almost pure" CH_4 multilayer just discussed, we find characteristic heat capacity peaks falling along the phase boundary between dense (1DS) and commensurate (1CS) solid monolayer phases found in Lysek's pure CH_4 study, indicating that the monolayer formed in dis-

placement has similar structure to that of pure CH_4 on bare graphite. This commensurability transition ("1DS-1CS," marked with a solid line in Fig. 1) can be traced back to lower $|\delta\mu_{CH_4}|^{-1/3}$ in the coadsorption system, well into the region where displacement is clearly incomplete and the film is mixed. In fact, the phase boundary extends down to CH_4 coverages of roughly 15% of the pure CH_4 monolayer density. The continuous displacement indicated by our film density measurements is thermodynamically incompatible with the scenario of a commensurability transition in a phase separated island of pure CH_4 covering 15% of the surface. It is possible that CH_4 "impurities" adsorbed into a primarily CCl_4 film form microscopic clusters with a locally pure CH_4 structure, even at low CH_4 coverage. The clusters must be large enough to display the commensurability transition as would a pure CH_4 solid, but small enough to prevent full phase separation from the CCl_4 film, with the composite solid likely stabilized by an entropy of mixing. While surprising, this result confirms the observation of Dupont-Pavlovsky,[7] discussed in the introduction, in which neutron scattering data indicate pure solid CH_4 domains emerging by 20% CH_4 coverage in the CH_4/CCl_4 coadsorption system, even though isotherm measurements indicate continuous displacement.

A pure CH_4 monolayer on graphite has phase boundaries separating dense solid (1DS), commensurate solid (1CS), expanded solid (1ES), and liquid (1L) phases. In the coadsorption system below displacement completion, however, we observe no heat capacity signal from either a CS-ES or melting transition. The absence of a melting signal indicates that the CH_4 giving rise to the coadsorption 1DS-1CS transition does not behave as pure CH_4 as we raise the temperature. As we increase $\delta\mu_{CH_4}$ towards displacement completion, however, a new calorimetry peak emerges around 103 K. The feature traces out a sharp first-order phase boundary ("new first-order transition," marked with a bold line in Fig. 1), snaking to lower and then higher temperatures as we increase coverage. Film coverage measurements show the coadsorption and single species isotherm curves joining at this curve, indicating that, from 100 to 104 K (and higher), displacement of CCl_4 becomes complete (or very nearly complete) along this new first-order phase boundary. The 1CS-1DS transition seems to "disappear" into the first-order phase boundary at higher $|\delta\mu_{CH_4}|^{-1/3}$, and both transitions vanish within the mixed phase at low CH_4 chemical potentials.

While the nature of the "mostly CH_4" film to the right of this first-order phase boundary is not clear, its CH_4 density is only a few percent less than that of pure CH_4 at the same $(T, \delta\mu_{CH_4})$. The nature of the corresponding heat capacity peak and its appearance several degrees below the pure CH_4 monolayer melting line suggest it is also associated with a melting transition, between a nearly pure CH_4 solid phase and a mixed liquid phase. From the melting point depression, caused by the entropy gained in forming a mixture, we would estimate a roughly 0.7% concentration of CCl_4 (by number) dissolved in the liquid phase, using the simple model described in the appendix. Associating this transition with melting is not without complication, particularly in light of another phase transition, with points marked with a star, appearing at the highest coverages; however, the simplest scenario remains that, in crossing to the low T side of this boundary, the film both solidifies and becomes nearly pure in CH_4.

This is the general picture of the CH_4/CCl_4 coadsorption phase diagram emerging from our measurements. The following sections will describe the experimental techniques (Sec. III) and detailed data (Sec. IV) used to draw these conclusions.

III. EXPERIMENTAL DETAILS

The experimental apparatus[17,18] and the techniques used for growing and studying coadsorbed films[12,19] are described in detail in previous publications. As such this section gives only a brief overview of the experimental arrangement and the details specifically relevant to the CH_4/CCl_4 measurements.

The measurements utilized a dedicated scanning ratio calorimetry apparatus designed for the study of the phase diagrams of multilayer physisorbed films on graphite.[17,18] The substrate is 29 g of Grafoam,[20] an uncompressed Grafoil with roughly 5 m^2 surface area per cc, in a cell with roughly 100 cc volume, yielding an adsorption surface area with $\sqrt{3} \times \sqrt{3}$ commensurate monolayer coverage $N_{\sqrt{3}}=165$ stpcc. In a calorimetry run, the sample cell is warmed by a precision heater controlled such that the cell temperature tracks that of a nearby copper "comparison" thermal mass, which is heated with a constant applied power. The sample cell heat capacity, and in particular the film contribution, are extracted from the cell heater data. This allows automated scanning of a wide temperature range, typically 70 to 115 K for this CH_4/CCl_4 study in roughly 1 day, with high sensitivity to any heat capacity peaks or anomalies corresponding to a phase transition or desorption in the film. Additionally, the sample cell is connected by a fill tube to a room temperature capacitive pressure gauge, allowing measurement of the film vapor pressure. At the temperatures studied here, the saturated vapor pressure of bulk solid CCl_4 is below 10^{-8} Torr, and so the measured pressure is to high precision the vapor pressure of the adsorbed CH_4. This allows direct calculation of the CH_4 chemical potential $\delta\mu_{CH_4}$ and, with accurate accounting of the total number of CH_4 molecules in the system, a volumetric measurement of the CH_4 film coverage number $N_{CH_4}^{film}$. The apparatus thus allows, for each of many runs performed with different CH_4 fillings, a dynamic scanning measurement of the coadsorbed film heat capacity $C(T, \delta\mu_{CH_4})$ and equation of state for the film CH_4 density $n_{CH_4}(T, \delta\mu_{CH_4})$.

The calorimetry data presented here are a subset of more than 100 calorimetry runs measured for coadsorbed CH_4/CCl_4 films and can be divided into two sets of data, both obtained on a single cooldown of the CCl_4 preadsorbate. The first subset, labeled "mecA," ("mec" as in methane coadsorption) explored the multilayer regime of film growth, using a quantity of methane equivalent to film coverages from 2–4 monolayers (or ML, to be defined shortly). The second dataset, "mecB," used CH_4 coverages in the range 0.01–2 ML, and was used in compiling the precision coadsorption isotherms that, along with similar data for Kr/CCl_4,

were used to verify a simple thermodynamic model for displacement in terms of the spreading pressure of the different film phases.[11]

The saturated preadsorbed monolayer was formed by room temperature adsorption of 430 stpcc of CCl_4—the equivalent of 5 monolayers, as the monolayer film density of CCl_4 (Ref. 21) corresponds to 82 stpcc in our cell–followed by a slow, multiday cooldown to liquid nitrogen temperatures (preadsorbate film growth is described in detail in Ref. 12). As CCl_4 forms only a single monolayer at temperatures below 217 K,[22] this excess filling ensures a full, saturated CCl_4 monolayer film in equilibrium with bulk CCl_4 crystals. Assuming that CH_4 would adsorb on any bare patch of graphite following the same equation of state that it would have in the absence of CCl_4, we can put an upper limit on the amount of graphite left bare by the preadsorption of CCl_4 by taking the ratio of the coadsorbed CH_4 coverage at the lowest $\delta\mu_{CH_4}$ (and thus at the lowest CH_4 coverage) and to the CH_4 coverage in the single species system at the same value of $(T, \delta\mu_{CH_4})$. Using the data in Fig. 3 (to be discussed shortly), the percentage of the graphite substrate left bare is seen to be less than 1%.

Introduction of CH_4, to grow the coadsorbed film, was performed in small doses between calorimetry runs, with a typical dose size of order 10% ML typically added to the system. This was followed by an "annealing" of the film at 120 K before a controlled cooldown and subsequent warming for calorimetry. For both datasets used here, the coadsorbed films were formed on the adsorption branch of CH_4 film growth to avoid coverage hysteresis associated with the nucleation of capillary condensate[23] in the pores of the graphite substrate. Though the saturated CCl_4 occupies a large portion of the pores and thus suppresses capillary condensation by the inert gas species, as demonstrated in the Kr/CCl_4 system,[12] forming films on the adsorption branch is still important for obtaining reliable film density measurements.

Two important "corrections," both necessitated by the limited mobility, and thus slow equilibration, of the CCl_4 preadsorbate, were applied to the data and merit discussion here. First, as has been repeatedly observed,[5–7,11,12] displacement of CCl_4 by a more volatile inert gas such as Kr or CH_4 does not run to completion in the exfoliated graphite substrates; the reduced step size associated with subsequent layers of inert gas adsorption following displacement indicates that inert gas adsorption occurs only on a fraction of the graphite substrate. Given its low vapor pressure and associated low mobility, it is likely that the displaced CCl_4 does not form the true macroscopic crystals dictated by equilibrium thermodynamics, which would occupy very little of the graphite surface area, but rather form quasibulk microcrystals locally, in such a way as to occupy a significant portion of the substrate area.[12] Empirically, we have observed, for a number of different cooldowns of preadsorbed CCl_4 and for both Kr and CH_4, that F^{-1}, the fraction of the surface area occupied by the displacing inert gas film, remains constant for an entire dataset, with the coadsorption film maintained on the adsorption branch of film growth, across the temperature range studied. F is defined, and experimentally determined, as the normalization factor by which one must multiply the inert gas (CH_4 in this case) coverage data $N_{CH_4}^{film}$ in order to overlap the isotherm data for the inert gas species on bare graphite at high chemical potentials, in the post-displacement coverage regime.

The factor F was measured to be 1.28 for the A coadsorption dataset and 1.48 for dataset B. The coverage data are thus accordingly normalized to give the CH_4 film density

$$n_{CH_4} = \frac{N_{CH_4}^{film}}{N_{\sqrt{3}}} F \tag{1}$$

in units of $\sqrt{3}\times\sqrt{3}$ monolayer coverage, or ML. While not reproducible between different cooldowns of the preadsorbed CCl_4 or between different coadsorbed film growths with an inert gas, the factor F has allowed reproducible measurements of film density n for both the Kr and CH_4 coadsorption systems. The "nominal normalized coverage" for a given run, used in the captions of various figures, is expressed in ML, normalized by the appropriate factor F, and includes all CH_4 molecules, film plus gas, sealed in the system for that run.

An additional correction was necessitated by the finite time for film-gas equilibration in the coadsorption system, which causes the film vapor pressures measured in a dynamic, temperature scanning, measurement to lag behind the true equilibrium values (this is also described in Ref. 12). This delay time is related to the slow dynamics of the CCl_4 moving between film and bulk crystal phases, but also to an observed delay in the flow of gas in and out of the sample cell. This latter delay was related to a partial CCl_4 plug at the mouth of the sample cell, where a cold spot likely formed during the initial cooldown of the preadsorbed film to allow an accumulation of CCl_4, which then remained frozen at the low temperatures of the experiment. Upon identification of this delay (between the A and B coadsorption datasets), we began to record the vapor pressure values for each experimental run on the cooling cycle as well as during the warming calorimetry cycle. Combined with a simple linear model for the relaxation of the pressure versus its equilibrium value (p_0),

$$\frac{dp}{dT} = -\frac{p - p_0(T, n_{CH_4})}{\tau(T, n_{CH_4})}, \tag{2}$$

where $\tau(T, n_{CH_4})$ is the relaxation time, which in general depends on temperature and film coverage. Combining the cooldown and warming cycle pressure data, one can use Eq. (2) to calculate the equilibrium vapor pressure value, as well as an estimate of the relaxation time, which ranged from as much as a half hour at the lowest temperatures and coverages to minutes at higher temperatures. The magnitude of the pressure correction, in terms of its impact on the calculated value of the CH_4 chemical potential $\delta\mu_{CH_4}$, ranged from $\Delta(\delta\mu_{CH_4}) \approx 15$ K at the lowest coverages to only several K at midrange temperatures and coverages. As the cooldown pressure data were only available for the mecB coadsorption dataset, only the B data have been corrected. The A dataset is only presented here at the high coverages, corresponding to 3-4 layers of CH_4, that were not covered by the B dataset,

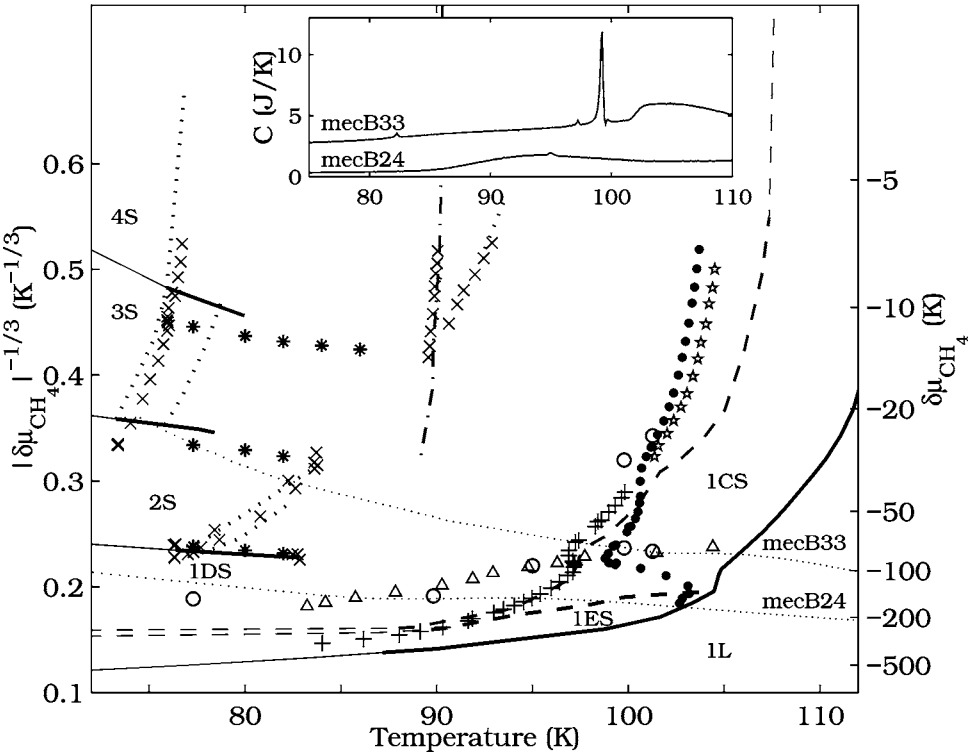

FIG. 2. Measured CH_4/CCl_4 phase boundary crossings (individual markers), plotted against the phase diagram for CH_4 on bare graphite (solid and dashed lines), as measured in the same cryostat (Refs. 13 and 17). The pure CH_4 monolayer has, in the temperature range of relevance to this study, dense (1DS), commensurate (1CS), and expanded (1ES) solid phases, in addition to a fluid phase (1L) (Refs. 13, 25, and 26). The upper layer regime displays first-order layering transitions (solid lines), layering critical points, and a complex melting behavior (dashed lines) (Ref. 13). The melting line for unsaturated capillary condensate (Ref. 23), approaching the 90.7 K bulk triple point, is traced "-·-." Pure CH_4 phase boundaries have been extended by linear extrapolation (thinner lines), where necessitated by the absence of measured data, to qualitatively illustrate the topology of the phase diagram, by extrapolation to the edges of the region plotted. For the coadsorption system, in the second and higher layers, first-order layering transitions are marked $*$ and calorimetry peaks are marked $\times$. The peak associated with the 1DS-1CS transition is marked $+$. A first-order transition associated with a new large and narrow calorimetry peak is marked ●. The low T edge of a broad desorption feature is marked △ and roughly coincides with displacement completion as defined by isotherm data, marked ○. A small, sharp feature observed just above the first-order transition is marked ★. Finally, two "experimental trajectories" (dotted line) illustrate the path in $(T, \delta\mu_{CH_4})$, followed by two typical runs (mecB24 and 33) crossing several coadsorption phase boundaries, accompanied in the inset by the corresponding heat capacity data.

where the pressure correction would have negligible impact on the measured phase boundaries and film coverage.

Finally, though only mildly relevant even at the lowest pressures and temperatures of this study, the film vapor pressure data, measured by a room temperature pressure gauge, have been corrected for thermal transpiration using the measured coefficients of Takaishi and Sensui.[24] For comparing the coadsorption system to the behavior of CH_4 on bare graphite, we use the calorimetry data from Refs. 13 and 17, which were measured in the same apparatus used here. This dataset is referenced as "mesA" ("s," single species), while additional CH_4 on bare graphite data at low coverages, measured as part of this present study, is referred to as "mesB." The CH_4 on bare graphite isotherm data used for comparison with the coadsorption coverage data has been measured both here and in Ref. 17.

Peaks in the heat capacity data give the first clues to the CH_4/CCl_4 coadsorption phase diagram. These are first identified in the calorimetry data and then associated with the corresponding chemical potential to give phase boundary points in $(T, \delta\mu_{CH_4})$. This is facilitated by the dual plots of heat capacity and chemical potential trajectories for a number of runs, as seen in Figs. 6, 9, and 10. In these plots, the heat capacity scans are plotted, from lowest to highest, in order of increasing coverage, with the scans displaced vertically in order to avoid overlap of the data. The chemical potential trajectories are not displaced and naturally fall in order of lowest to highest coverage.

The locus of heat capacity peaks and other features are plotted in the $(T, \delta\mu_{CH_4})$ plane in Fig. 2 for all runs of the two main coadsorption datasets, along with the phase boundaries measured in the pure CH_4 adsorption system. These heat capacity features can be correlated with the simultaneously measured film equation of state data, $n_{CH_4}(T, \delta\mu_{CH_4})$. These are plotted as isotherms, along with isotherm data for CH_4 on bare graphite at the same temperatures, in Fig. 3, where the coadsorption isotherms have been constructed by "slicing" the film coverage data for many successive runs at different CH_4 fillings at the desired isotherm temperature. The corresponding CH_4 on bare graphite data, both in terms of heat capacity and film coverage, provide the necessary backdrop against which the coadsorption

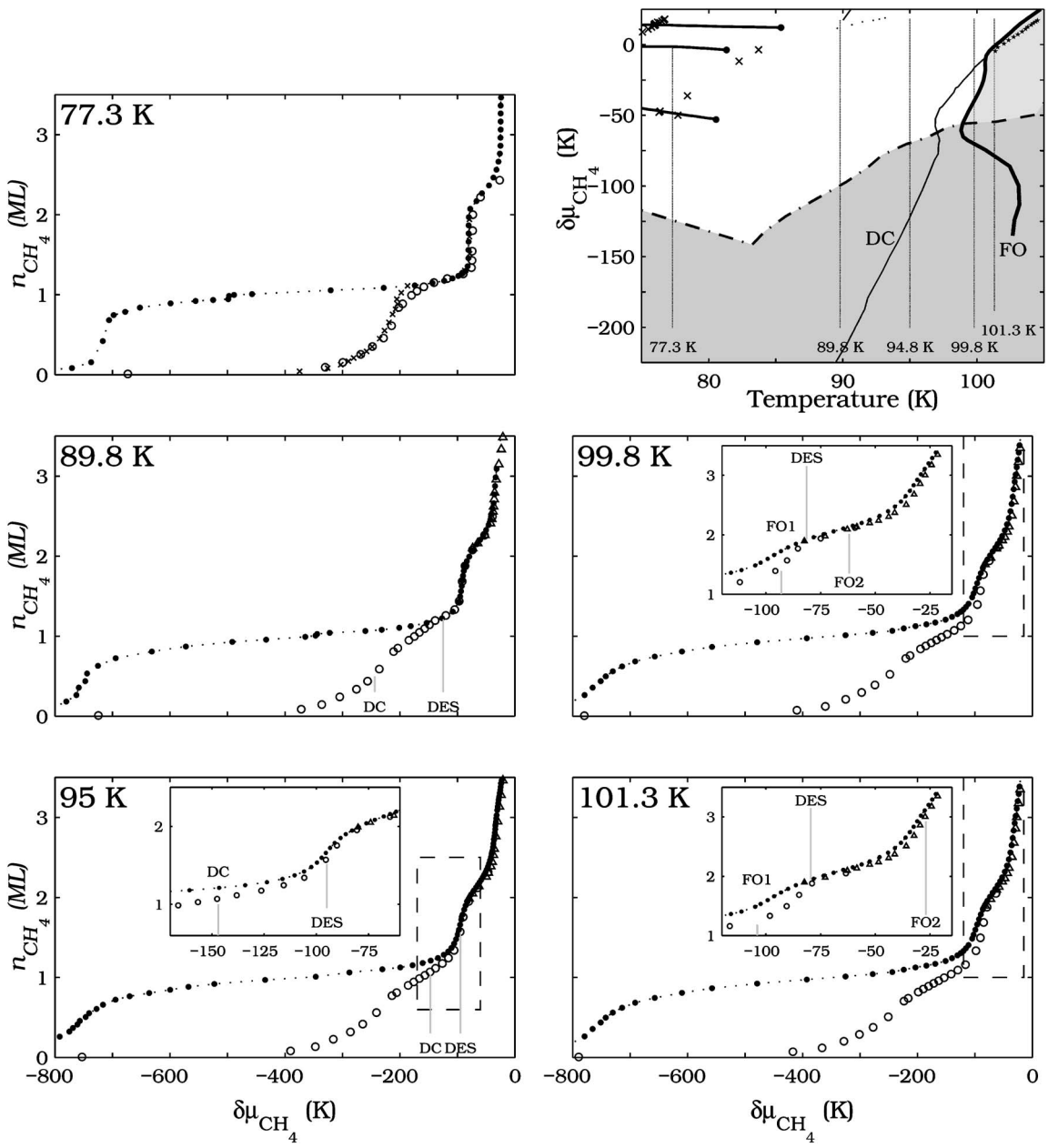

FIG. 3. Single species (●) and coadsorption (from cooldown B, marked ○, and, at higher coverages, cooldown A, marked △) isotherm data at 77.3, 89.8, 95, 99.8, and 101.3 K. A scale factor F equal to 1.27 and 1.48 has been used for cooldowns A and B, respectively. Coadsorption data are measured with the dynamic technique described in Sec. III. At 77.3 K, the dynamic data are accompanied by data measured with a static, fixed temperature technique (marked ×), for which $F=1.75$. The schematic figure at top right shows the portions of the phase diagram "sliced" by these isotherms. In the isotherm data, the lines marked "DES," "DC," and "FO" designate the values of $\delta\mu_{CH_4}$ at which one finds heat capacity features associated with, respectively, the onset of desorption as displacement is reversed, the 1DS-1CS commensurability transition, and a new coadsorption first-order phase transition described in Sec. IV D (as this boundary is crossed twice at some temperatures, these crossings are marked "FO1" and "FO2," in order of increasing chemical potential). The CH_4 single species data at 95 K are taken from Lysek (Ref. 17), and the lowest pressure data points at 77.3 K are as reported by Thomy and Duval (Ref. 27); all other data were measured as part of this study and that of Ref. 11.

phase diagram is studied, allowing, particularly in the post displacement, high CH_4 coverage regime, a test of the degree to which the coadsorbed film behaves similar to CH_4 on bare graphite. The detailed discussion of the experimental results in the next section will refer often to the data in these two figures.

Equilibration aspects, particularly the assignment of equilibrium thermodynamic concepts such as the equation of state and heat capacity to dynamically measured experimental quantities, are a legitimate source of concern in a coadsorption system with a limited mobility preadsorbate such as CCl_4. These issues are discussed at length for Kr/CCl_4 in

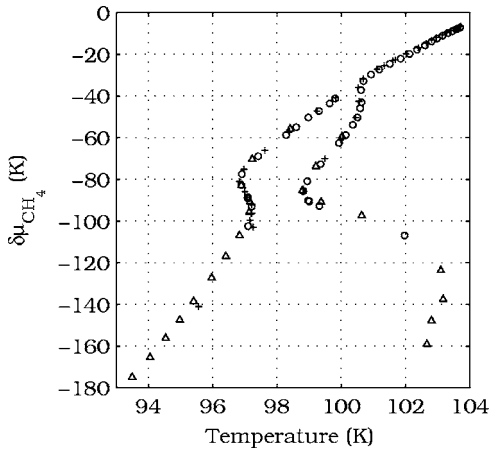

FIG. 4. Comparison of the location in $(T, \delta\mu_{CH_4})$ for heat capacity peaks corresponding to the crossing of two different phase boundaries for three different datasets: ○ for mecA, △ for mecB, and + for a third exploratory dataset, measured prior to mecA. The two phase boundaries—the colder a monolayer commensurability transition and the warmer a new observed first-order transition—are discussed in Secs. IV A and IV D.

Ref. 12. That displacement of CCl_4 is achieved only on a portion of the graphite surface is itself an example of nonequilibrium behavior, as is the observed nonreproducibility of the fraction of surface area F^{-1} undergoing displacement, for repeated growths of the "same" coadsorbed film. However, the measured film phase boundary locations in $(T, \delta\mu_{CH_4})$ and the film density equation of state $n_{CH_4}(T, \delta\mu_{CH_4})$, are reproducible, at a level comparable to the experimental uncertainties, even for different film growths with different values of F. Figure 4 shows the close overlap of data from the A and B coadsorption datasets, in addition to a third exploratory dataset, for two important phase transitions to be discussed in Secs. IV A and IV D. Despite the difficulty in distributing CCl_4 around the entire cell in order to form true macroscopic crystals that would free up the graphite surface for full displacement, CCl_4 does enter and exit the film phase reversibly on experimental time scales, as seen both in the coverage data and in the CH_4 desorption heat capacity peaks, that accompany the reversal of displacement (Sec. IV B). Additionally, the dynamic measurement technique is observed to have little impact on the results. This is seen for the film density, in Fig. 3, in the consistency of the 77.3 K dynamically measured isotherm data with data measured using a standard static isothermal dosing technique. The dynamically measured heat capacity is reproducible for different scan rates, seen in Fig. 5, even upon crossing through a region of displacement and a first-order phase transition. Such observations, similar to those made for Kr/CCl_4, suggest that equilibrium thermodynamics adequately describe the essential aspects of the CH_4/CCl_4 coadsorption, indicating that a local equilibrium, including the exchange of CCl_4 molecules between film and bulk solid phases on experimental time scales, occurs.

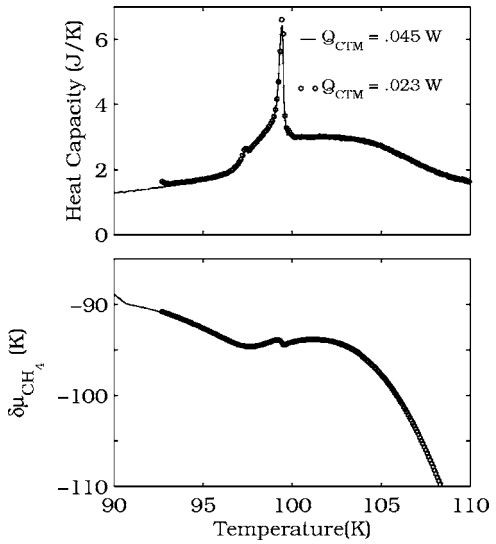

FIG. 5. Comparison of heat capacity runs, and the corresponding trajectories in $(T, \delta\mu_{CH_4})$, performed at two different heating rates, for roughly 2 ML CH_4 coverage. The 45 mW power applied to the comparison thermal mass is the nominal rate used in all other measurements and produces a scan rate of roughly 2 K/h, while 23 mW scans at roughly half that rate. The reproducibility in the measurements indicates the validity of the dynamic measurement technique, at least for the scan rates employed, even upon crossing a first-order phase boundary (discussed in Sec. IV D).

IV. EXPERIMENTAL RESULTS FOR COADSORBED CH_4/CCl_4

A. Low CH_4 coverage data: Onset of CH_4 order in a mixed film

Figure 6 shows the heat capacity traces for low CH_4 coverages, in addition to the experimental trajectories in $(T, \delta\mu_{CH_4})$. A small, sharp feature emerges near 84 K in the mecB09 dataset, at a normalized CH_4 coverage near 15% of a CH_4 monolayer (0.15 ML). It is not seen in the preceding run with CH_4 density of roughly 0.09 ML. The peak moves to higher temperatures with increasing coverage and is superimposed, for runs mecB21 and higher, on a broad heat capacity feature that we will associate, in the following section, with CH_4 desorption upon reversal of displacement. Referring to Fig. 7 (or Fig. 2), with increasing CH_4 coverage the location of the feature traces out a curve (marked +) in $(T, \delta\mu_{CH_4})$ that roughly merges into the phase boundary traced, in the pure CH_4 adsorption system (denoted "--" in the figure), between solid phases that are, respectively, DS and CS with the underlying graphite lattice substrate.[13,25] Likewise, as seen in Fig. 7, the peak in the coadsorption system is similar, in shape and magnitude, to the 1DS-1CS peak in the single species adsorption system. It is thus reasonable to associate this peak in the coadsorption system with the 1DS-1CS commensurability transition occurring in the coadsorbed film.

If the assignment of this small peak to the 1DS-1CS commensurability transition is correct, it is remarkable that we observe it for such small CH_4 coverages in the middle of a continuous displacement transition, which, as discussed ear-

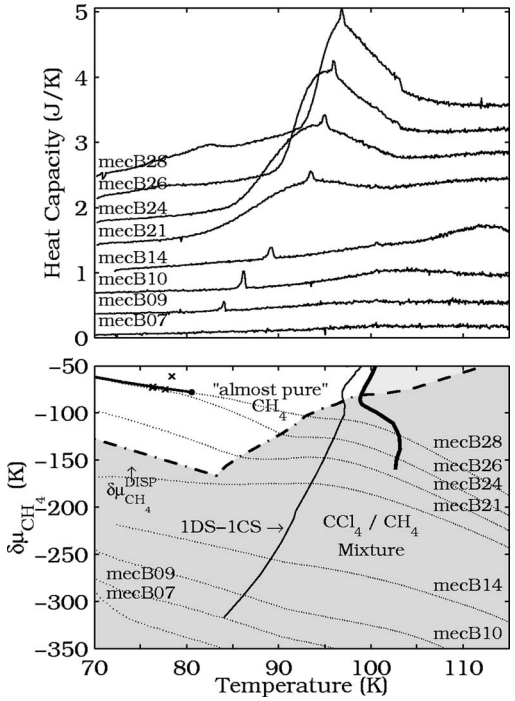

FIG. 6. Heat capacity (top) and chemical potential (bottom) trajectories for calorimetry scans at low CH_4 coverage. Runs 7, 9, 10, 14, 21, 24, 26, and 28 from the mecB dataset are shown (nominal normalized coverages of 0.09, 0.15, 0.25, 0.45, 1.05, 1.21, 1.35, and 1.56 ML). Heat capacity traces have been displaced vertically, here and in subsequent heat capacity figures, to avoid overlap in the data.

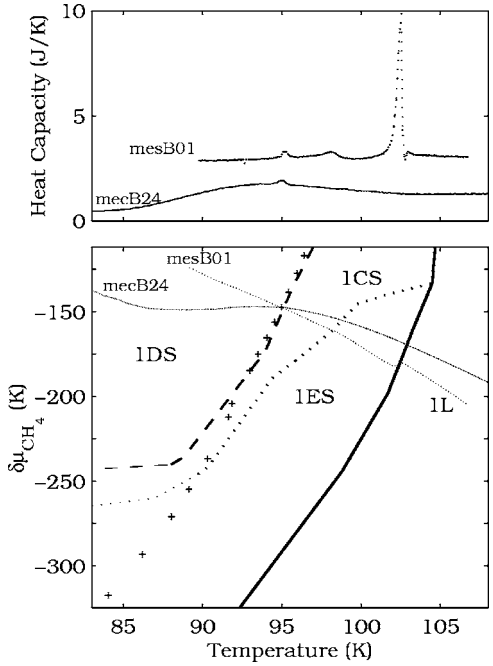

FIG. 7. Comparison of heat capacity (top) and chemical potential (bottom) data between roughly monolayer coverages of CH_4 in the coadsorption (solid) and single species (dotted) systems. The monolayer phase boundaries for pure CH_4 are plotted as solid and dashed lines, while the heat capacity peaks likely associated with the dense to commensurate (1DS-1CS) transition in the coadsorption system are marked +. The pure CH_4 data show three monolayer phase transitions, while the coadsorption data displays only the 1DS-1CS feature, in addition to a broad calorimetry feature associated with desorption in the coadsorption system (Sec. IV B).

lier, implies a single mixed CH_4/CCl_4 phase. This is seen clearly in the CH_4 coverage data in Fig. 3 at, for instance, 89.8 K, where the chemical potential of the 1DS-1CS phase boundary (marked DC) is seen to correspond to roughly 50% ML CH_4 coverage, right in the middle of the continuous displacement process. This surprising observation actually confirms the neutron scattering data of Dupont-Pavlovsky and co-workers[7] and will be discussed again in Sec. V A.

While the presence of the heat capacity signal associated with the 1DS-1CS transition implies CH_4 order within the mixed CCl_4/CH_4 phase present during displacement, other transitions associated with pure CH_4 on bare graphite are not observed in the coadsorption system. As shown in Fig. 7, for pure CH_4, the 1DS-1CS transition is followed at these coverages by heat capacity peaks[13,26] corresponding to a second solid-solid transition (between commensurate and expanded phases) and finally a first-order melting transition. Signals associated with 1CS-1ES phase transition and, particularly, with first layer melting, are conspicuously absent from these coadsorption measurements for CH_4 coverages below the completion of displacement.

B. Crossing the displacement completion phase boundary: Calorimetry as displacement is reversed

In addition to the peak from the 1DS-1CS transition, the coadsorption calorimetry data show a very broad heat capacity maximum, clear in mecB21 (Fig. 6) and becoming larger and better defined as coverage is increased in subsequent runs. The low temperature onset of these peaks, as quantified by the temperature in which the second derivative of the heat capacity reaches a maximum—at 83 K in mecB24 and moving to higher temperature with increasing CH_4 coverage—are marked Δ in the $(T, \delta\mu_{CH_4})$ plane in Fig. 2. The curve traced by these heat capacity points coincides roughly with the position in $(T, \delta\mu_{CH_4})$, marked $\bigcirc$, of displacement completion at 89.8 and 95 K, where the coadsorption isotherm data join the corresponding film density for CH_4 on bare graphite. This correspondence is also visible in the isotherm data in Fig. 3, where the chemical potential values corresponding to the peak onset at the same temperatures are marked "DES." Referring to the proposed phase diagrams in Figs. 1 and 6, these broad heat capacity features can thus be associated, at least below 99 K, with the desorption of CH_4 that occurs as the system passes from the post-displacement "almost pure CH_4" into the lower $\delta\mu_{CH_4}$ "CCl_4/CH_4 mixture" phase. The corresponding proposed displacement completion phase boundary, $\delta\mu_{CH_4}^{disp}(T)$, is traced here with "-·-."

The broad heat capacity feature is largely explained by the heat capacity of desorption accompanying the increase in CH_4 desorption that occurs when the system slips into the mixed film phase and displacement is "run in reverse," with CCl_4 reclaiming the graphite surface. This increased desorption is seen in the slight turn towards higher $\delta\mu_{CH_4}$, seen in

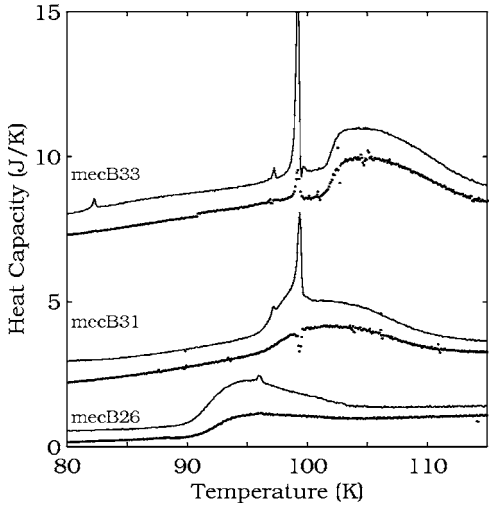

FIG. 8. Heat capacity (solid) and heat capacity due to desorption (dotted) for coadsorbed CH_4/CCl_4, at nominal normalized CH_4 coverage of 1.35, 2.02, and 2.47 $\sqrt{3}\times\sqrt{3}$ monolayers. The heat of desorption is calculated using $\frac{\partial\mu}{\partial T}|_N$ evaluated from our own coverage dataset (Ref. 19).

runs mecB24, 26, and 28 in Fig. 6, upon crossing the proposed displacement completion phase boundary; this "upwards turn" means a larger rate of increase of the film vapor pressure and thus a larger rate of desorption to populate the CH_4 gas phase. Removing CH_4 from bound film states into the gas takes energy, with a corresponding contribution to the heat capacity proportional to the rate of desorption from the film, $C_{\rm des}=-q_D(dN^{\rm film}_{CH_4}/dT)$, where

$$q_D = T\left[\left(\frac{\partial\mu^f}{\partial T}\right)_{N^{\rm film}_{CH_4}} - \left(\frac{\partial\mu^g}{\partial T}\right)_{N^{\rm gas}_{CH_4}}\right]. \quad (3)$$

The heat of desorption q_D can be evaluated from the dataset for the coadsorbed film coverage $n_{CH_4}(T,\delta\mu_{CH_4})$.[19] Figure 8 shows heat capacity scans plotted with the calculated desorption heat capacity for several coadsorption runs. In each case, the broad feature coincides with a similar feature in the heat capacity contribution from desorption, confirming the identification of the peak with desorption. That the desorption contribution does not completely account for the the broad peak, at least for mecB26 and mecB31, indicates that there is some additional entropy increase as the mixture composition changes and the film restructures. While displacement is continuous at these temperatures, with no vertical step in the coadsorption isotherm, the sharp onset of the desorption feature suggests association of a phase boundary with displacement completion. The other peaks present in the heat capacity in Fig. 8—particularly the small peak near 82 K in mecB33 and the large, sharp peak near 99 K in mecB31 and 33—are the subjects of Secs. IV C and IV D, respectively.

C. Low temperature, high CH_4 coverage data: Alterations to the pure CH_4 multilayer phase diagram

The isotherm data in Fig. 3 show that CH_4 displacement of CCl_4 at low temperatures results in a film that, as in the Kr/CCl_4 case, closely obeys the film density equation of state for the inert gas species on bare graphite. However, unlike Kr, for which the post-displacement multilayer phase diagram is identical to that of pure Kr,[12] the CH_4/CCl_4 calorimetry data reveal significant departure from the pure CH_4 multilayer phase diagram, indicating that the film formed by displacement is not simply pure CH_4 (hence the title "almost pure CH_4" given to the high coverage, low temperature portion of the proposed coadsorption phase diagram in Fig. 1).

Figure 9 shows heat capacity and experimental trajectory data in the multilayer coadsorption regime. The trajectories converge, for different coverages, along the formation of the second, third, and fourth layers of CH_4, indicating first-order layering transitions. These phase boundaries correspond to the chemical potential locations of vertical steps in the coadsorption isotherms, which are marked here with an asterisk, at 1 K intervals). The larger asterisks represent possible layering critical endpoints, roughly estimated as the temperatures at which the reciprocals of the the higher temperature (supercritical) isotherm slopes $(\partial N^{\rm film}_{\rm meth}/\partial\delta\mu_{CH_4})^{-1}_T$, extrapolate to zero. Also marked 'by ×' are the low temperature heat capacity peaks in the coadsorption system. For the second layer, a broad heat capacity feature is visible near 83 K (runs mecB28-30) and coincides roughly with the point at which the experimental trajectories separate, with the isotherm slopes thus becoming measurably finite,[28] likely signaling the passage near the second layering critical point, not far from where it is observed in the pure CH_4 system.

As seen in Fig. 2, the chemical potentials of layer 3 and 4 formation are several K below the layer condensation levels in the pure CH_4 system. However, it should be noted that these higher coverage data are uncorrected for the finite equilibration time and are thus systematically lowered by at least several K. As such, we cannot conclude that these upper layering transitions in the coadsorption system are truly shifted with respect to their counterparts in the pure CH_4 system.

A clear difference between the coadsorption and pure CH_4 systems arises in the second layer disordering, illustrated in Fig. 9. The pure CH_4 second layer melting line joins the second layering transition at a 77.7 K triple point. A second phase boundary precedes melting by 2–3 K, giving rise to two heat capacity peaks and two phase boundaries moving in parallel to higher temperatures and higher coverage. Both heat capacity features vanish in the vicinity of third layer condensation. While the nature of the lower temperature phase boundary is not known, one reasonable possibility is a commensurability transition in the second layer, relative to the first layer, before melting.[13]

The coadsorption system also shows a second layer triple point, with a sharp peak appearing at 76.3 K in mecB29 and then growing larger at the same point in $(T,\delta\mu_{CH_4})$ in subsequent higher coverage runs. The triple point temperature, however, is almost 1.5 K below the pure CH_4 second layer triple point, and, additionally, there is no evidence of a second heat capacity peak. The second layer in the coadsorption system thus crosses only one phase boundary in disordering. The absence of the second phase transition (and thus the disappearance of a phase in the second layer) indicates that the bilayer film formed after displacement in the coadsorp-

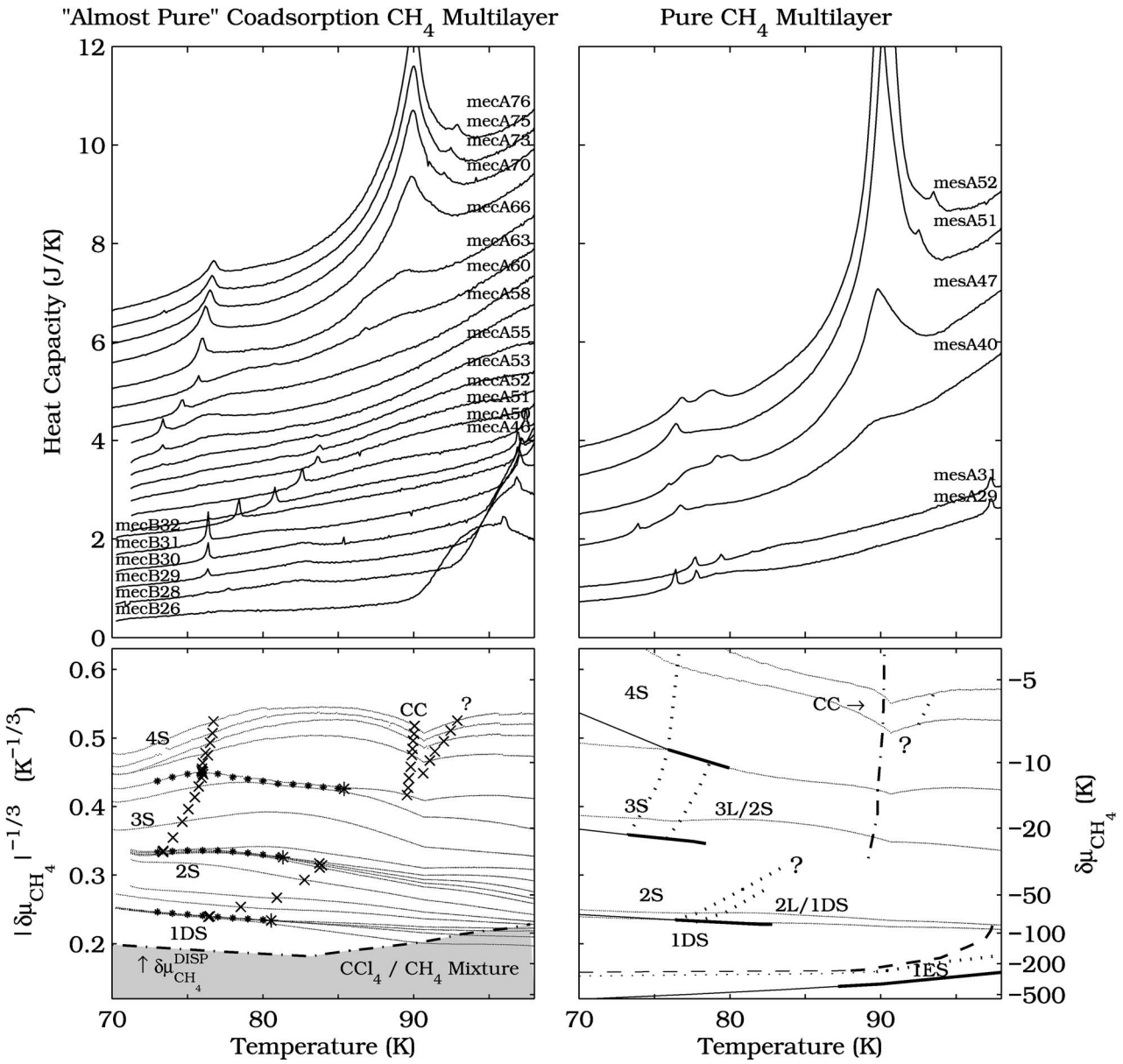

FIG. 9. Coadsorption heat capacity (top left) and chemical potential (bottom left) data for scans in the second, third, and fourth layers in CH_4/CCl_4. Runs mecB26, 28, 29, 30, 31, and 32 have nominal coverages of 1.36, 1.56, 1.68, 1.82, 2.02, and 2.24. Runs mecA46, 50, 51, 52, 53, 55, 58, 60, 63, 66, 70, 73, 75, and 76 have coverages of 2.32, 2.45, 2.61, 2.67, 2.78, 2.93, 3.19, 3.59, 4.14, 4.77, 5.97, 6.62, 7.01, and 7.39 ML. Pure CH_4 calorimetry and chemical potential data are shown on the right for comparison (Ref. 17). The left and right tick labels for $|\delta\mu_{CH_4}|^{-1/3}$ and $\delta\mu_{CH_4}$ apply to both the coadsorption and single species phase diagrams.

tion system is not simply pure CH_4 on graphite. It is possible that the substrate for second layer growth—the first layer—is not pure CH_4 and alters the relative stability of the different second layer phases. Another possibility is that a small amount of CCl_4 mixes into the liquid phase of the "mostly CH_4" second layer, such that the lower temperature, solid-solid phase transition observed for pure CH_4 is preempted by a melting transition which has been pushed to lower temperatures by the mixing entropy in the liquid phase. The true nature of the film phases in the second layer for CH_4 on bare graphite is not well understood, and this also complicates any interpretation of the coadsorption bilayer.

As coverage is increased near to third layer formation, this heat capacity peak, likely associated with disordering of the second layer is seen, in Fig. 9 to become smaller and finally disappear. The two phase transitions in the pure CH_4 system also disappear with higher coverage. Note that the disappearance of the heat capacity feature, near $T=83.5$ K and $|\delta\mu_{CH_4}|^{-1/3}=0.32$ $K^{-1/3}$, occurs very near the point at which the experimental trajectory curves passing through the third layer condensation line begin to diverge, and thus in proximity of the third layer critical point. It thus appears possible that the second layer melting and third layer condensation lines join at the third layer critical point. If the phase boundaries actually do come together, it would imply that first-order condensation of the third layer is only possible on top of an ordered second layer. It would also imply that the second layer cannot be solid above 83.5 K, well

below the bulk methane triple point of 90.7 K. The disappearance of the second layer melting signal in the pure CH_4 film was not well understood and it is not clear whether this interpretation would be possible for the pure system as well. In contrast, the second layer pure Kr and Ar melting curves both extend to temperatures well above their bulk triple points.[29,30]

The third and fourth layer phase diagrams for coadsorbed CH_4/CCl_4 also show clear departure from the behavior of pure CH_4 multilayer films. As with the second layer, the pure CH_4 third layer experiences two phase transitions in going from a low temperature solid to a liquid, with a lower temperature phase boundary observed several degress below the melting line. The lower temperature phase boundary appears to merge with the fourth layer triple point.[13,17] In the coadsorption system, the third layer displays a triple point and melting line (runs mecA50 and higher in Fig. 9), but, as with the second coadsorption layer, shows no evidence of a second, lower temperature transition. With increased coverage, third layer melting appears to tie in with the fourth layer. The connection of the third and fourth layers is similar to the pure CH_4 system, except that here it is the phase boundary extending from the third layer triple point that connects to the fourth layer triple point, rather than a second, lower temperature third layer transition.

The large, broad peak near 90 K seen in Fig. 9 for mecA63 and subsequent runs is associated with the melting of unsaturated capillary condensate, as in the pure CH_4 system.[23] There is also a small peak observed just above the broad capillary condensate (CC) melting peak (marked 'with a question mark' in the coadsorption phase diagram), visible at roughly 92 K in mecA73 and in following runs. This feature was also observed in the pure CH_4 data (runs mesA47 and 51), where the peak seemed to disappear into the larger CC peak.[17] The origin of this phase boundary for pure CH_4 was not clear; it does not obviously connect to any phase boundary on the low T side of capillary condensate melting, and it seems unlikely that it would be related to some change in the capillary condensate liquid phase. In the coadsorption system, this heat capacity peak falls on the same phase boundary as in the pure film. Additionally, as observed in the Kr/CCl_4 system, the excess preadsorbed CCl_4 successfully fills the pores in the graphite substrate, which significantly reduces the amount of capillary condensed CH_4 and thus also the relative magnitude of the CC melting peak (runs mecA75 and mesA51 have similar CH_4 coverages, but the coadsorption system has a much smaller CC melting peak). The reduced CC melting peak makes this transition more visible, particularly at the low coverage side where it runs into the CC melting peak. As the peak can be more clearly seen to not connect to other phase boundaries in the multilayer film, our observation here only renders this peak more mysterious.

D. High temperature, intermediate CH_4 coverage data: Displacement completion in a new first-order phase transition above 100 K

A new heat capacity feature, not observed in the pure CH_4 system, is first observed as a small "right shoulder" on the broad desorption feature near 103 K in mecB28 (see Fig. 10), occurring within the mixed CCl_4/CH_4 phase before displacement completion. This feature sharpens into a peak as it moves to *lower* temperature with increasing coverage (run mecB31). The peak grows and sharpens, tracing out a phase boundary (marked with a bold solid line in Fig. 10), that drops to near 99 K before turning towards higher temperatures with increasing coverage. The sharp peak thus "passes through" to the low temperature side of the broad desorption

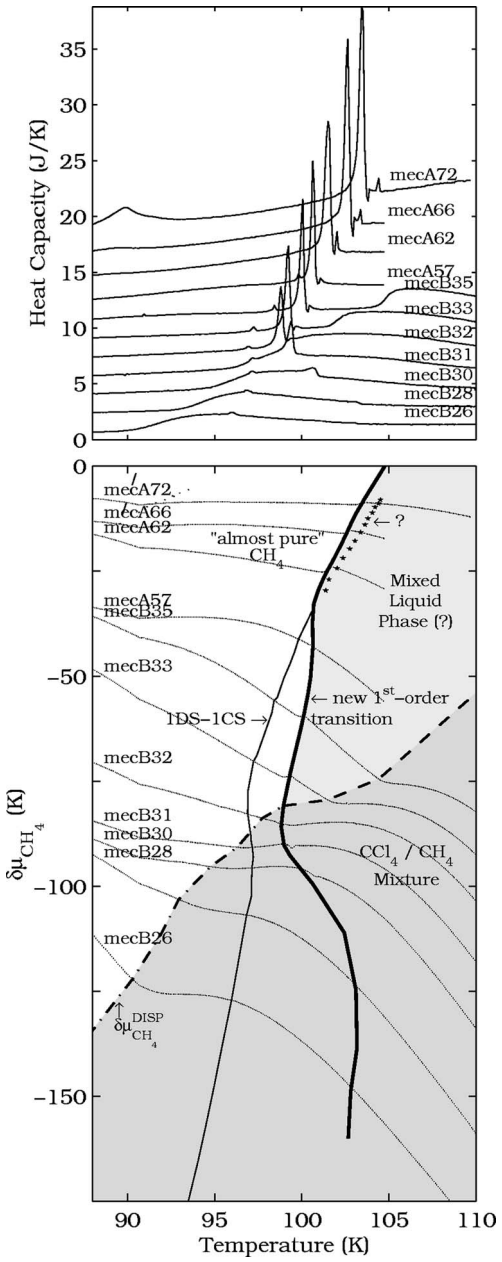

FIG. 10. Heat capacity (top) and chemical potential (bottom) trajectories indicating the onset of a new first-order phase transition. Runs shown are mecB26, 28, 30, 31, 32, 33, 35 (nominal CH_4 coverages of 1.36, 1.56, 1.82, 2.02, 2.24, 2.47, and 2.74 $\sqrt{3}\times\sqrt{3}$ monolayers) and mecA57, 62, 66, and 72 (coverages 3.02, 3.95, 4.77, and 6.28). The broad peak near 90 K in mecA72 corresponds to the melting of unsaturated capillary condensate and is discussed in Sec. IV C.

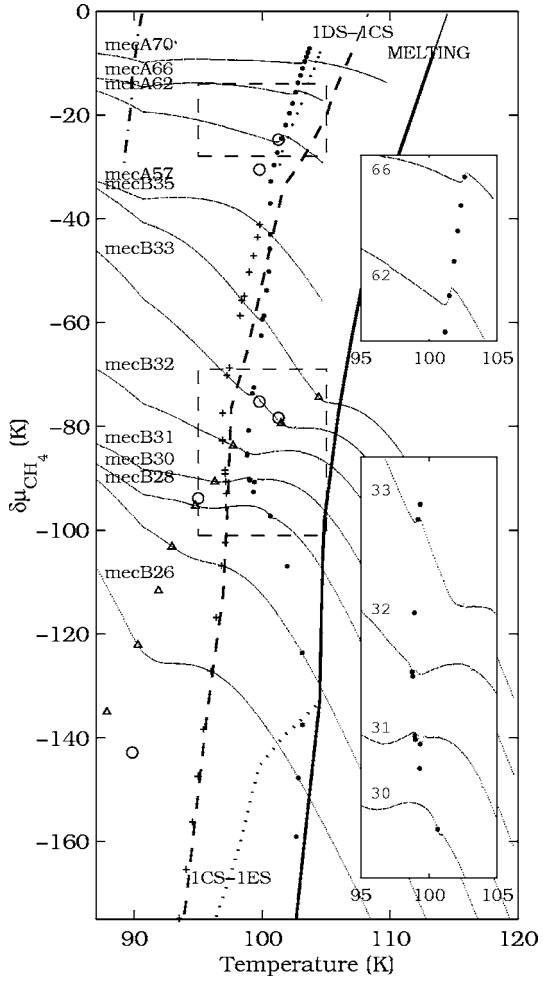

FIG. 11. Trajectories in $(T, \delta\mu_{CH_4})$ crossing the new first-order phase boundary (marked ●), plotted against the extended monolayer phase diagram for pure CH_4. Other coadsorption features are marked as in Fig. 2. Insets expand the $\delta\mu_{CH_4}$ axis to highlight the system's movement along the first-order phase boundary. Nominal $\sqrt{3}\times\sqrt{3}$ coverages are 1.36, 1.56, 1.82, 2.02, 2.24, 2.47, and 2.74 monolayers for mecB and 3.02, 3.95, 4.77, and 5.97 for mecA. The dash-dot phase boundary at the upper left corresponds to the capillary condensate melting curve.

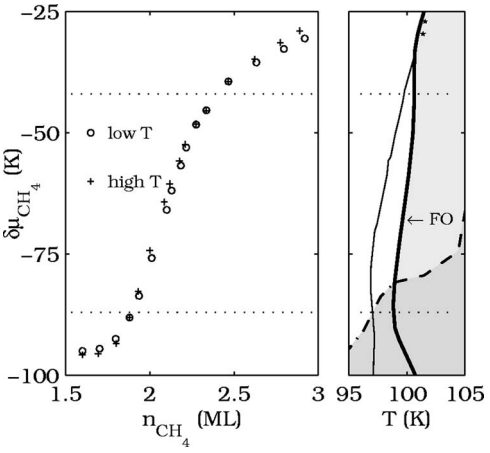

FIG. 12. CH_4 film densities (plotted along the x axis) as a function of chemical potential on the high (+) and low (○) temperature sides of the first-order phase boundary. Lines at $\delta\mu_{CH_4}=-87$ and −42 K roughly indicate where $\frac{d\delta\mu_{CH_4}}{dT}$ becomes infinite along the phase boundary and the density discontinuity vanishes.

feature, which moves to higher temperatures and traces a nearly horizontal line in Fig. 10 (marked with a dashed line above 99 K). The small heat capacity feature identified with the 1DS-1CS transition in Sec. IV A is seen to merge into this large heat capacity peak (last seen in mecB35), after having first moved to the low temperature side of the phase boundary traced by the analogous transition in the pure CH_4 system (this is marked "+" in Fig. 11). We will associate this dominant sharp feature in the CH_4/CCl_4 calorimetry data with a first-order phase transition that coincides with the completion of displacement for temperatures above 99 K.

Figure 11 shows the experimental trajectories in $(T, \delta\mu_{CH_4})$ upon crossing the phase boundary traced out by this line of heat capacity peaks (marked •). Note that the trajectories experience a distinct "glitch" along the boundary (most obvious in the insets expanding the $\delta\mu_{CH_4}$ axis). The temperature width of the heat capacity peaks corresponds roughly to that of the experimental trajectory glitches. The large heat capacity peak thus represents a first-order phase transition, with the system moving along the phase boundary to resolve a density discontinuity between the two phases.

At higher coverages, where $d\delta\mu/dT$ along the phase boundary is positive, the system moves "up" the phase boundary, to higher $\delta\mu_{CH_4}$, and thus desorbing CH_4 before moving completely into the lower density high temperature phase. This is seen clearly in, for instance, run mecB33 or, at higher coverage, run mecB62 in Fig. 11, particularly in the inset. This is typical behavior for a film system moving into a higher temperature phase of lower density, with the system desorbing as it moves "up" the phase boundary to higher pressures, before moving into the high temperature phase. For $\delta\mu_{CH_4}\approx -100$ K, however, the slope $d\delta\mu/dT$ is negative along the phase boundary, and the system thus moves "down" the phase boundary (observed for runs mecB30 and 31). Here, lower chemical potential means lower CH_4 gas pressure, less CH_4 desorption, and thus a higher density than if the film stayed in the lower temperature phase. This serpentine behavior of the phase boundary, passing from positive to negative slope (passing through the vertical) is rather unique among studied adsorption systems.

Figure 12 plots the CH_4 densities on the low (○) and high (+) T sides of the phase boundary.[31] The density discontinuity can be appreciated in the horizontal separation of the two density curves at a given value of $\delta\mu_{CH_4}$ and results to be as small as perhaps −0.1 ML at the lowest coverages and nearly 0.2 ML at the highest coverages (where positive implies that the low temperature phase is denser than the higher temperature phase). Note that the two phases have equal density for $\delta\mu_{CH_4}\approx -90$ K and for $\delta\mu_{CH_4}\approx -40$ K, which are both points in which the phase boundary slope $d\delta\mu_{CH_4}/dT$ becomes infinite. A generalized coadsorption Clausius-Clapeyron equation, relating density discontinuity and phase boundary slope to latent heat, permits a phase boundary of infinite slope *only* for vanishing density discontinuity (see

the Appendix), and thus this observation is consistent with general thermodynamic requirements. In similar fashion, the serpentine path taken by the phase boundary likely reflects density changes in the low temperature phase related to the formation of the second and third layers of film growth.

These positive (and negative) density discontinuities upon crossing this first-order phase boundary result in positive (and negative) desorption heat capacity contributions. This is seen in Fig. 8 where runs mecB31 and mecB33 have desorption heat capacity contributions of opposite sign upon crossing the phase transition. That the desorption contributions do not nearly account, in either case, for the size of the large heat capacity peak shows that there is a true film entropy difference in crossing to the higher temperature phase, a restructuring of the film rather than just desorption.

A comparison between the curve in $(T, \delta\mu_{CH_4})$ traced by this phase boundary and the coadsorption isotherm data at 101.3 K allows association of this first-order phase transition with displacement completion at these high coverages. Upon crossing the phase boundary, the film CH_4 density approaches that of CH_4 on bare graphite. The points marked ○ in Fig. 11 denote the locations in $(T, \delta\mu_{CH_4})$ at which the coadsorption isotherm curves join the single species data within our experimental resolution. The 90 and 95 K displacement completion points have already been associated with the onset of the desorption feature (marked △). At 99.8 K and, more clearly, at 101.3 K, there are instead two values of $\delta\mu_{CH_4}$ (and thus two "○" markers) for which the coadsorption CH_4 density reaches that of CH_4 on bare graphite, the first corresponding to the onset of the broad desorption feature and the second upon crossing the new first-order phase boundary. This is also seen in the isotherm data in Fig. 3, where, at 101.3 K (see inset), the coadsorption and single species isotherm data are observed to join, within the experimental resolution, twice.[32] The coadsorption curve first joins the pure CH_4 data around $\delta\mu_{CH_4} \approx -80$ K, then separates, and finally reapproaches[33] around $\delta\mu_{CH_4} \approx -25$ K. These two points correspond roughly with the desorption onset and first-order heat capacity features, which are labeled DES and FO2 in the isotherm inset. There is another, lower coverage crossing of the curving first-order boundary at 101.3 K (marked FO1 in Fig. 3), but this occurs well below the completion of displacement and thus is not relevant to this discussion.

Displacement, at temperatures above 100 K, can thus be viewed as terminating in a first-order phase transition. Approaching this first-order phase boundary from "below," from the side of low $\delta\mu_{CH_4}$, there is continuous CH_4 adsorption up to the point, marked "--" in Figs. 10 and 1, and corresponding to the onset of the desorption heat capacity figure, where the CH_4 coverage is very nearly that of CH_4 on bare graphite. With increasing $\delta\mu_{CH_4}$, however, the CH_4 density once again falls below that of pure CH_4 on bare graphite, likely indicating a mixture phase, before reaching the first-order phase boundary. The nature of the phase on the high T, lower CH_4 coverage side of this phase boundary is not clear, except that its density is slightly lower than for a pure CH_4 film at the same point in $(T, \delta\mu_{CH_4})$, indicating that it is likely a mixed phase. However, the first-order nature of the

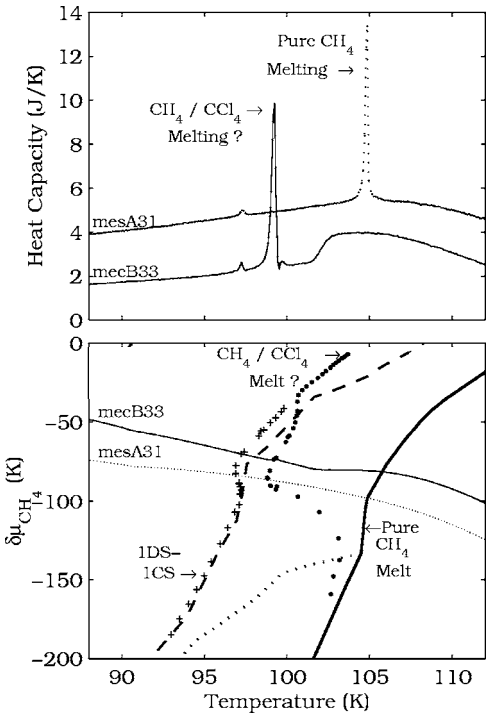

FIG. 13. Comparison of the melting transition in a pure CH_4 monolayer with the sharp first-order phase transition in coadsorbed CH_4/CCl_4.

phase boundary and the location, size, and shape of the heat capacity peak, when compared to the pure CH_4 data (see Fig. 13) suggests that this new first-order coadsorption phase boundary may be associated with melting into a mixed liquid film phase. Recalling the reduced melting point of salt water, the first-order phase transition in the coadsorption system could move to a lower temperature because the entropy of mixing associated with the CCl_4 impurity increases the stability of the liquid phase. The observation of the 1DS-1CS transition and agreement with the pure CH_4 coverage data suggest that the coadsorbed film has a relatively pure CH_4 solid monolayer below the phase boundary (with any higher layer coverage likely disordered around 85 K, as discussed in Sec. IV C), and one would certainly expect the monolayer to melt at some point. Associating the coadsorption first-order transition with melting is thus a simple and logical hypothesis.

A simple model relating the melting point depression ΔT_M to a given impurity concentration of the preadsorbate, n_1 is given in the Appendix and yields

$$\Delta T_M = -\frac{n^{\mathrm{liq}}_{CCl_4} k_B T}{(n^S_{CH_4} - n^L_{CH_4}) \dfrac{d\delta\mu^{\mathrm{liq:sol}}_{CH_4}}{dT}}, \tag{4}$$

at a fixed value of $\delta\mu_{CH_4}$, where $n^S_{CH_4}$, $n^L_{CH_4}$, and $\frac{d\delta\mu^{L:S}_{CH_4}}{dT}$ refer to CH_4 densities and the slope of the melting curve in the pure CH_4 system. Equation (4) assumes a weak solution of an impurity in the liquid phase perturbing the phase boundary with a pure solid film.

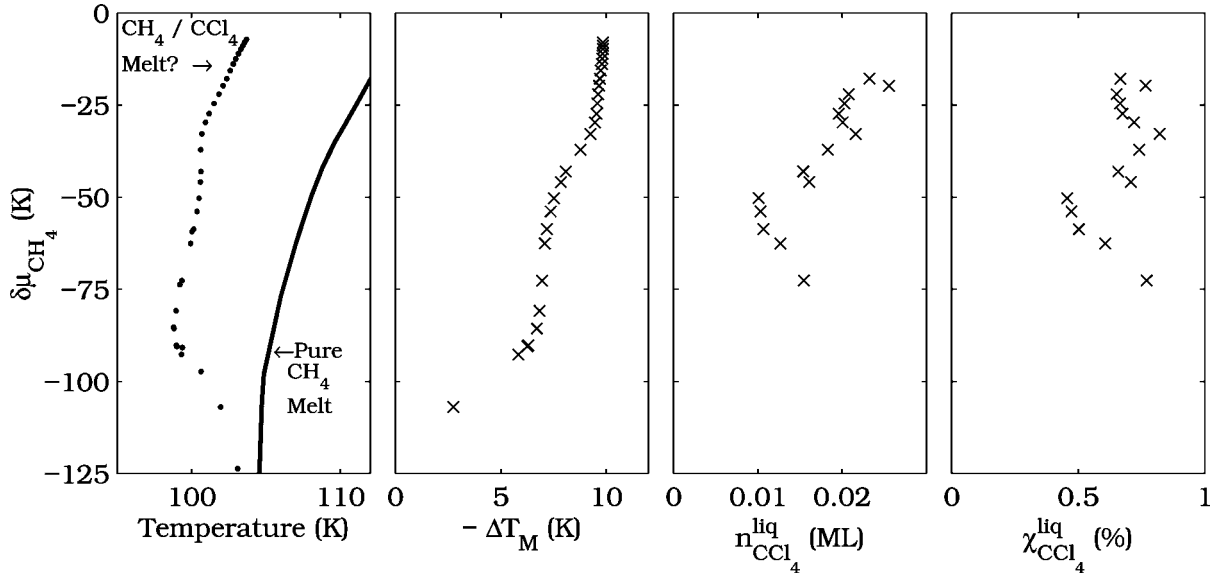

FIG. 14. Pure CH_4 and (proposed) mixed CH_4/CCl_4 melting boundaries, with data for the melting point depression ΔT_M, CCl_4 impurity density $n^{\mathrm{liq}}_{CCl_4}$, and impurity concentration $\chi^{\mathrm{liq}}_{CCl_4}$. Note that the units for $n^{\mathrm{liq}}_{CCl_4}$ are $\sqrt{3}\times\sqrt{3}$ monolayers [a pure CCl_4 monolayer would have a density of roughly 0.5 in these units (Ref. 21)].

We can estimate $n^{\mathrm{liq}}_{CCl_4}$, the impurity concentration of CCl_4 in the mixed liquid phase, from the other terms in Eq. (4), all of which are measureable. ΔT_M is simply the temperature difference between the coadsorption and pure CH_4 melting curves (see Fig. 14). From Lysek's pure CH_4 data, we can calculate the pure film density discontinuity.[34] Results of this calculation, for $n^{\mathrm{liq}}_{CCl_4}$ and the impurity concentration by number, $\chi \equiv n^{\mathrm{liq}}_{CCl_4}/n^{\mathrm{liq}}_{CH_4}$, are shown in Fig. 14. This is only an approximate calculation, mainly due to the interpolation of the coarsely spaced melting density discontinuity data in the pure CH_4 system, which introduces scatter of up to 30% in the data. No calculation is made for $\delta\mu_{CH_4} < -80$ K, where our pure CH_4 data along the phase boundary are too sparse to allow reasonable interpolation of the density discontinuity.

Our melting point depression data suggest an impurity concentration of CCl_4 in the liquid film phase between 0.5 and 1% by number along the proposed melting boundary. This simple model assumes a lower temperature phase that is pure solid. However, if both liquid and solid phases contained small amounts of CCl_4 impurity, then the calculation presented here would yield the *difference* in the amount of CCl_4 in the two phases.

Observation of a small heat capacity feature appearing just above the temperature of the large first-order peak raises a significant counterpoint to this interpretion of a mixed liquid phase. Referring to Fig. 10, this small, sharp peak is observable in mecA62, 66, and 72, tracing out a phase boundary marked by stars in Fig. 10. While calorimetry temperature control imperfections can produce a slight "bounce" in the calorimetry data following a sharp peak, observed to some degree in all runs from mecB33 on in Fig. 10, the signal in runs mecA66 and following cannot be explained as an experimental artifact; the calorimetry data has settled before the smaller peak is observed, and the small peak moves away from the large first-order feature with increasing coverage. The peak's shape and location in $(T, \delta\mu_{CH_4})$ are consistent with a high coverage extension of the 1DS-1CS phase boundary that seemed to "disappear" into the striking first-order phase boundary, between runs mecA57 and 62 in Fig. 10. If the phase boundary marked by stars is truly an extension of the 1DS-1CS transition, our association of the first-order phase transition with monolayer melting is very likely incorrect, as a mixed liquid phase should not undergo a solid-solid commensurability transition. Even if unrelated to the 1DS-1CS transition, a similar heat capacity peak would not be expected to follow a monolayer melting transition.

V. CONCLUSIONS

Perhaps the most interesting question addressed by this study is how a pure solid monolayer of CCl_4 evolves continuously, as indicated by the coadsorption isotherm data, into a film that has a CH_4 density comparable to that of CH_4 on pure graphite. The detailed calorimetry study presented here give some important clues but no simple answers to this question. Our concluding comments focus on two aspects of this issue.

A. CH_4 order in the midst of continuous displacement

At CH_4 coverages as low as 0.15 ML, where isotherm data indicate that the system is in the middle of continuous displacement of CCl_4 from the graphite surface, a heat capacity peak is observed, corresponding in size, shape, and location in $(T, \delta\mu_{CH_4})$ to the phase boundary associated with the 1DS-1CS commensurability transition for CH_4 on bare graphite. As continuous displacement, occurring over a range of $\delta\mu_{CH_4}$, rules out, by the Gibbs phase rule, phase separation of pure CH_4 and pure CCl_4 domains (or even of separate CH_4- and CCl_4-rich phases), it is surprising to observe a

solid-solid phase transition characteristic of pure CH_4. Nonetheless, our observation confirms, and extends to a wider temperature range, the neutron scattering data of Dupont-Pavlovsky *et al.*[7] who observe a dense monolayer solid CH_4 scattering peak emerging at similar low coverages in the midst of continuous displacement of CCl_4 at 77 K. These authors also note the thermodynamic incongruity of the observation.

It is tempting to dismiss these observations, on the ground that perhaps, due to the limited low temperature mobility of CCl_4, some portions of the graphite surface behave independently and do not "feel" the presence of CCl_4, thus allowing pure CH_4 adsorption and its associated heat capacity signals from its phase transitions. However, this scenario would leave an even bigger mystery—why do these pure CH_4 domains not melt or display the 1CS-1ES transition observed for pure CH_4? The absence of the low coverage melting transition is thus a further confirmation of the isotherm data measured here and elsewhere,[7] that imply that there is no true phase separation of CH_4 in the displacement transition.

One hypothesis that is consistent with both the thermodynamic requirement that continuous displacement be a single phase process and the apparent observation of a transition between two ordered solid phases is that the CH_4 forms its own microscopic domains within the CCl_4 monolayer. These domains would correspond to clusters of CH_4 large enough to locally display the order that pure CH_4 would have at a given $(T, \delta\mu_{CH_4})$ on bare graphite (and give rise to the observed solid CH_4 2D neutron scattering signal and 1DS-1CS transition), yet small enough to enjoy some thermodynamic advantage that prevents macroscopic phase separation from the CCl_4 and, consequently, melting. The film would grow continuously in CH_4 as the number of patches diverges and CH_4 substitutes CCl_4 in a single solid phase. The entropy gained by remaining in small clusters could stabilize the CH_4 islands against macroscopic phase separation. Another possibility is that there is some energetic advantage to creating CH_4-CCl_4 interfaces in the film (in effect, a negative line tension). It is worth noting that the pure CCl_4 monolayer has roughly half the number density of monolayer CH_4, so continuous displacement cannot occur on a "one for one" basis; on average, two CH_4 molecules must replace a single CCl_4 molecule. This may encourage formation of the proposed CH_4 clusters.

Such a scenario is indeed surprising and seems to demand a rather delicate free energy balancing act to stabilize a homogeneously mixed phase with ordered CH_4 islands, a single phase evolving continuously from a pure CCl_4 monolayer into a nearly pure solid CH_4 film. That is, however, what the data from two experiments, using different techniques, seem to suggest, and the issue could merit theoretical and computational attention.

B. New first-order phase boundary: First-layer melting into a mixed liquid phase?

Displacement at higher temperatures in the CH_4/CCl_4 system seems to be completed by a first-order phase transition, analogous to the behavior observed above 112 K for the Kr/CCl_4 system.[12] The form of the heat capacity peak and its position in $(T, \delta\mu_{CH_4})$ suggest that this first-order phase transition is associated with melting of the pure CH_4 (or nearly pure CH_4) monolayer into a mixed liquid film phase. Thus, at temperatures above 100 K, the CCl_4 monolayer continuously evolves, with increasing $\delta\mu_{CH_4}$, into a CH_4-rich liquid film arriving at multilayer thickness, with the monolayer finally solidifying, forming a nearly pure CH_4 solid substrate for second and higher liquid layers, with a total CH_4 coverage similar to that of pure CH_4 on bare graphite. A similar scenario could also be consistent with the Kr/CCl_4 system, but the monolayer melting transition occurred at temperatures exceeding the useful range of our apparatus, and so a proper investigation was not possible. The measured depression in the melting temperature here corresponds to a concentration of CCl_4 in the mixed liquid phase of roughly 1%, by number, along the phase boundary (or, if both solid and liquid phases contain CCl_4 impurities, a 1% excess in the liquid phase concentration).

The case for this interpretation of the observed first-order phase transition is weakened somewhat by the observation of the heat capacity feature corresponding to the phase boundary, marked by stars in Figs. 1 and 10, observed at high coverages on the high-temperature side of the observed first-order phase transition. A possible connection, as its position suggests, to the 1DS-1CS commensurability transition, would be incompatible with the proposed mixed liquid phase. Additionally, the crossing of one film phase boundary by another in a quadruple point would be incompatible with the Gibbs phase rule. Assuming, on the other hand, that this other phase boundary is unrelated to the 1DS-1CS phase transition, one is still left with the mysterious presence of this small peak above the first-order phase transition, inside what should be a liquid film phase.

In spite of the observation of this heat capacity peak, the association of this new first-order phase transition with monolayer melting into a mixed liquid remains the simplest and most likely interpretation. This hypothesis could be tested in different ways. A structural experiment, analogous to the 77 K neutron scattering study cited here,[7] could investigate whether the monolayer solid order really disappears upon heating the system across the phase boundary measured here. An alternative, possible in a calorimeter such as that employed here, would be to measure the CH_4 monolayer melting curve as a function of the trace quantity of CCl_4, added to the system as an impurity, to see if the impurity really serves to gradually lower the melting point. Such a technique would approach the coadsorption of an inert gas on graphite with a highly condensable species, such as CCl_4 from a different angle, in which the preadsorbed CCl_4 saturation is approached from "below," starting with very small amounts of CCl_4.

APPENDIX: THERMODYNAMIC ANALYSIS OF MELTING TO A DILUTE MIXTURE LIQUID FILM

As in bulk thermodynamic systems, such as salt water, the melting point of a solid film can be reduced by the presence of impurities that mix predominantly into the liquid phase,

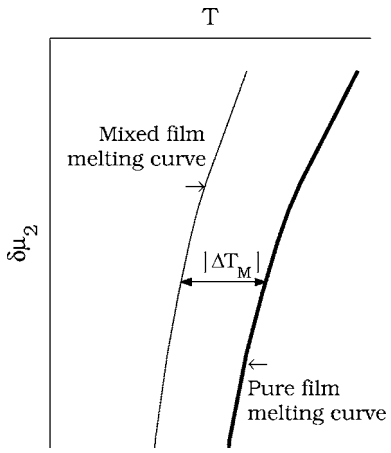

FIG. 15. Illustration of the melting phase boundary in the pure film of species 2 (heavy solid line) and for a coadsorption system with a mixed liquid phase (lightweight solid line), where a small quantity of the preadsorbate dissolves into the liquid phase of the inert gas film. The anticipated depression of the melting point, at a fixed value of $\delta\mu_2$, is $|\Delta T_M|$.

which is stabilized by the increased entropy provided by the solute. We study here the impact of a dilute impurity (of species 1) on the melting transition of an inert gas (species 2) film, as a function of chemical potential, $\delta\mu_2$, and the areal impurity concentration in the mixed liquid phase, $n_1 \equiv N_1/A$ (the solid phase is assumed to be purely species 2). This will allow determination of n_1 from the measured shift in the position of the melting curve in the $(T, \delta\mu_2)$ plane, as illustrated in Fig. 15. We thus treat the coexistence of a mixed liquid film phase (denoted "mix") with a pure solid film (denoted "S"), where the mixed phase is treated as a perturbation of the pure liquid phase (denoted L).

It will be useful to define the surface energy function ψ, given by

$$\psi \equiv E - TS - \mu_2 N_2, \tag{A1}$$

where S and E are the entropy and internal energy. The first law of thermodynamics can then be expressed as

$$d\psi = -SdT - \phi dA + \mu_1 dN_1 - N_2 d\mu_2, \tag{A2}$$

where ϕ is the film spreading pressure and A the film area. By extensivity of the energy function ψ, we see that $\psi = -\phi A + \mu_1 N_1$ and obtain the two component film Gibbs-Duhem relation

$$SdT - Ad\phi + N_1 d\mu_1 + N_2 d\mu_2 = 0. \tag{A3}$$

Equations (A1)–(A3) are valid both for the entire film system and for each individual film phase.

For phase coexistence, the solid phase and mixed liquid phases will share the same spreading pressure $\phi^S = \phi^{\text{mix}}$. The introduction of the surface energy ψ facilitates calculation of the spreading pressure

$$\phi^{\text{mix}} = -\left(\frac{\partial \psi^{\text{mix}}}{\partial A}\right)_{T,\mu_2,N_1} \tag{A4}$$

as a perturbation of the spreading pressure that the pure liquid phase would have ϕ^L in the absence of the impurity. The discussion that follows proceeds analogously to that used by Landau and Lifshitz[35] for bulk solutions.

For the mixed liquid phase, we assume that the solution is so weak that the solute molecules do not interact with one another, and thus only contribute to the surface energy ψ^{mix} with a term proportional to the number of particles $N_1\alpha(T, \mu_2, A)$ and an entropy related term owing to the indistinguishability of the solute molecules

$$\psi^{\text{mix}}(T, N_1, \mu_2, A) = \psi^L(T, \mu_2, A) + N_1\alpha(T, \mu_2, A) + k_B T \ln N_1! \tag{A5}$$

In the limit $\ln N! \approx N \ln \frac{N}{e}$, ψ can be reexpressed as a manifestly extensive surface energy

$$\psi^{\text{mix}}(T, N_1, \mu_2, A) = -\phi^L(T, \mu_2)A + N_1 k_B T \ln n_1 + N_1 k_B T \ln \beta(T, \mu_2), \tag{A6}$$

where

$$\frac{\beta(T, \mu_2)}{A} \equiv \frac{1}{e} \exp \frac{\alpha(T, \mu_2, A)}{k_B T}.$$

Simple differentiation with respect to A yields the spreading pressure in the mixed phase

$$\phi^{\text{mix}}(T, N_1, \mu_2) = \phi^L(T, \mu_2) + n_1 k_B T. \tag{A7}$$

The dilute solute thus adds an ideal gas-like contribution to the pure liquid film equation of state.

Phase coexistence is defined by the melting line where the spreading pressures of the (pure) solid and (mixed) liquid phases are equal. Written in terms of the temperature shift $\Delta T_M \equiv (T_M^{\text{mix}} - T_M)$ of the melting line, as a function of the solute chemical potential relative to bulk saturation $\delta\mu_2$,

$$\phi^S(T + \Delta T_M, \delta\mu_2) = \phi^{\text{mix}}(T + \Delta T_M, \delta\mu_2, n_1). \tag{A8}$$

Expanding in ΔT_M and n_1,

$$\phi^S(T, \delta\mu_2) + \left(\frac{\partial \phi^S}{\partial T}\right)_{\delta\mu_2} \Delta T_M = \phi^L(T, \delta\mu_2) + \left(\frac{\partial \phi^L}{\partial T}\right)_{\delta\mu_2} \Delta T_M + \left(\frac{\partial \phi^{\text{mix}}}{\partial n_1}\right)_{T,\delta\mu_2} n_1. \tag{A9}$$

This can be regrouped to yield $\Delta T_M(n_1)$ at a given fixed $\delta\mu_2$,

$$\Delta T_M = -\frac{n_1 \left(\frac{\partial \phi^{\text{mix}}}{\partial n_1}\right)_{T,\delta\mu_2}}{\left[\left(\frac{\partial \phi^L}{\partial T}\right)_{\delta\mu_2} - \left(\frac{\partial \phi^S}{\partial T}\right)_{\delta\mu_2}\right]}. \tag{A10}$$

The right-hand side in Eq. (A10) is always negative: the mixed film equantion of state [Eq. (A7)] allows expression of the numerator as $n_1 k_B T$, which is positive, and the de-

nominator must be positive in order to ensure that, on both sides of the phase boundary, the more stable phase has greater spreading pressure and thus minimizes the free energy.[36] As such, ΔT_M is negative and thus corresponds to a lowered melting point.

Reexpressing Eq. (A10) in terms of experimentally accessible quantities, we rewrite the Gibbs-Duhem relation [Eq. (A3)] for a film phase that is pure in species 2

$$d\phi = \left(s^i + n_2^i \frac{d\mu_2^0}{dT} \right) dT + n_2^i d\delta\mu_2, \tag{A11}$$

where $\mu_2 = \mu_2^0 + \delta\mu_2$ and areal entropy density $s^i \equiv \frac{S^i}{A}$.

From Eq. (A11), it follows that

$$\left(\frac{\partial \phi}{\partial T} \right)_{\delta\mu_2} = s^i + n_2^i \frac{d\mu_2^0}{dT}.$$

Finally, $d\phi^S = d\phi^L$ along the pure species 2 melting curve, and thus, again using Eq. (A11),

$$(s^L - s^S) + (n_2^L - n_2^S)\frac{d\mu_2^0}{dT} = (n_2^S - n_2^L)\left(\frac{d\delta\mu_2}{dT} \right)^{L:S}, \tag{A12}$$

where $\left(\frac{d\delta\mu_2}{dT}\right)^{L:S}$ is the slope of the pure species 2 melting curve. Substitution of these two results into Eq. (A10) yields the simple final result

$$\Delta T_M = -\frac{n_1 k_B T}{(n_2^S - n_2^L)\left(\frac{d\delta\mu_2}{dT} \right)^{L:S}}. \tag{A13}$$

Equation (A13) could also be modified for the general case of weak solubility of species 1 in both the solid and liquid phases, simply by replacing n_1 with $(n_1^L - n_1^S)$.

For this study, $(n_2^S - n_2^L)$ and $\left(\frac{d\delta\mu_2}{dT}\right)^{L:S}$ are obtained from the location in $(T, \delta\mu_{CH_4})$ of the pure CH_4 monolayer melting curve and the solid and liquid film coverages along this phase boundary. These thermodynamic arguments alone cannot predict whether the preadsorbate will form a solution, weak or strong, in either the liquid or solid phase of the inert gas species film. However, they do yield a simple estimation of the concentration of species 1 in a mixed phase, which is in practice difficult to measure, from the experimentally measured melting point depression ΔT_M and the pure species 2 melting curve data. As such, the measured coadsorption phase boundaries can give quantitative information for the composition of a possible mixed film phase.

An additional relevant expression can be obtained by developing Eqs. (A11) and (A12) for a first-order transition between two phases (a and b) of arbitrary, not necessarily pure, composition. This yields a generalized Clausius-Clapeyron relation along the phase boundary

$$(n_2^a - n_2^b)\left(\frac{d\delta\mu_2}{dT} \right)^{a:b} = (s^a - s^b) - (n_1^a - n_2^b)\left(\frac{d\mu_1}{dT} \right)^{a:b} - (n_2^a - n_2^b)\left(\frac{d\mu_2^0}{dT} \right)^{a:b}. \tag{A14}$$

For the coadsorption systems studied here, the preadsorbate species 1 (CCl_4 in our case) is at bulk saturation, and thus $\frac{d\mu_1}{dT} = \frac{d\mu_1^0}{dT}$, which is finite. Thus the entire right side of Eq. (A14) is finite, and so the only way for the phase boundary to have infinite slope $\left[\left(\frac{d\delta\mu_2}{dT}\right)^{a:b} = +\infty\right]$ is for species 2 (in our case CH_4) in the two phases to be equal. Thus, for the first-order phase transition discovered here for the CH_4/CCl_4 coadsorption system, the observation that the points along the phase boundary where the CH_4 density discontinuity goes to zero are also points where the slope $\left(\frac{d\delta\mu_2}{dT}\right)^{a:b}$ becomes infinite is in fact a requirement for thermodynamic validity.

*Present address: Dipartimento di Fisica, Università di Trento, Via Sommarive 14, 38050 Povo (TN), Italy.

[1] M. Bouchdong, J. Menaucourt, and A. Thomy, J. Phys. (France) **47**, 1797 (1986).
[2] A. Razafitianamaharavo, N. Dupont-Pavlovsky, and A. Thomy, J. Phys. (France) **51**, 91 (1990).
[3] A. Razafitianamaharavo, P. Convert, J. Coulomb, B. Croset, and N. Dupont-Pavlovsky, J. Phys. (France) **51**, 1961 (1990).
[4] J. Menaucourt and C. Bockel, J. Phys. (France) **51**, 1987 (1990).
[5] M. Abdelmoula, T. Ceva, B. Croset, and N. Dupont-Pavlovsky, Surf. Sci. **272**, 167 (1992).
[6] H. Asada, S. Doi, and H. Kawano, Surf. Sci. Lett. **273**, L403 (1992).
[7] N. Dupont-Pavlovsky, M. Abdelmoula, S. Rakotozafy, J. P. Coulomb, B. Croset, and E. Ressouche, Surf. Sci. **317**, 388 (1994).
[8] H. Asada, M. Takechi, and H. Seiyama, Surf. Sci. **346**, 294 (1996).
[9] H. Asada, H. Seiyama, and M. Takechi, Adsorp. Sci. Technol. **15**, 271 (1997).
[10] M. A. Castro and R. K. Thomas, Surf. Sci. **399**, 212 (1998).
[11] W. J. Weber and D. L. Goodstein, Phys. Rev. Lett. **83**, 3888 (1999).
[12] W. J. Weber and D. L. Goodstein, Phys. Rev. B **66**, 165419 (2002).
[13] M. J. Lysek, M. A. LaMadrid, P. K. Day, and D. L. Goodstein, Phys. Rev. B **47**, 7389 (1993).
[14] G. D. Halsey, J. Chem. Phys. **16**, 931 (1948).
[15] T. L. Hill, J. Chem. Phys. **15**, 767 (1947).
[16] W. A. Steele, *The Interaction of Gases with Solid Surfaces* (Pergamon Press, Oxford, 1974).
[17] M. J. Lysek, Ph.D. thesis, California Institute of Technology, Pasadena, 1992.
[18] M. J. Lysek, P. Day, M. A. LaMadrid, and D. L. Goodstein, Rev. Sci. Instrum. **63**, 5750 (1992).
[19] W. J. Weber, Ph.D. thesis, California Institute of Technology, Pasadena, 2000.
[20] Grafoam samples were provided by Union Carbide.
[21] P. W. Stephens and M. F. Huth, Phys. Rev. B **32**, 1661 (1985).

[22] M. Abdelmoula, T. Ceva, B. Croset, and N. Dupont-Pavlovsky, Surf. Sci. **274**, 129 (1992).
[23] M. Lysek, M. LaMadrid, P. Day, and D. Goodstein, Langmuir **9**, 1040 (1993).
[24] T. Takaishi and Y. Sensui, Trans. Faraday Soc. **59**, 2503 (1963).
[25] P. Vora, S. K. Sinha, and R. K. Crawford, Phys. Rev. Lett. **43**, 704 (1979).
[26] H. K. Kim, Q. M. Zhang, and M. H. W. Chan, Phys. Rev. B **34**, 4699 (1986).
[27] A. Thomy and X. Duval, J. Phys. I **67**, 1101 1970).
[28] The sparse spacing, in terms of CH_4 coverage, of our experimental runs causes an uncertainty of perhaps 2 K, a systematic underestimating, in our calculation of the critical temperatures at which the reciprocal isotherm slope becomes infinite. As such, the broad heat capacity maximum (near 83 K) is consistent with the 81 K critical point determined by the isotherm data.
[29] P. Day, M. LaMadrid, M. Lysek, and D. Goodstein, Phys. Rev. B **47**, 7501 (1993).
[30] P. Day, M. Lysek, M. LaMadrid, and D. Goodstein, Phys. Rev. B **47**, 10716 (1993).
[31] These densities are calculated by extrapolating each scan's coverage data on either side of the heat capacity peak up to the line connecting the heat capacity maxima. The actual trajectories do not pass exactly along this infinitesimal phase boundary line, but rather along and through a thin transition zone with a temperature width of a few tenths of a degree
[32] A similar comparison is also allowed by with the 99.8 K data, and the appropriate data are shown in Figs. 3 and 11. However, the first-order phase boundary is nearly vertical in $(T, \delta\mu_{CH_4})$ at this temperature, which renders separation of the points corresponding to the desorption onset, first-order heat capacity peak, and isotherm joining quite difficult. The 101.3 K data allows a much cleaner separation.
[33] Comparison of the pure CH_4 and coadsorption isotherm curves becomes problematic at film coverages of three or more layers because of capillary condensation, which in the coadsorption system is suppressed with respect to single species CH_4. Specifically, this results in a slight suppression of the coadsorption coverage with respect to that measured at high coverages in the pure CH_4 system, which is likely visible already in the high coverage data at 101.3 K in Fig. 3. Likewise, because the first-order phase boundary climbs steeply in coverage with increasing temperature and thus enters the regime where capillary condensate has a significant impact on isotherm data, we have not pursued the single species CH_4 isotherm data necessary to confirm the coincidence of displacement completion with the first-order phase boundary at even higher temperatures.
[34] As with the coadsorption system, the densities along the phase boundary for pure CH_4 are calculated by extrapolating a run's coverage on either side of the heat capacity peak to the phase boundary line connecting the heat capacity maxima for adjacent runs. The density curves are then interpolated to given values of the chemical potential and subtracted to give a density discontinuity $\Delta n_{CH_4}(\delta\mu_{CH_4})$.
[35] L. D. Landau and E. M. Lifshiftz, *Statistical Physics* (Pergamon, Oxford, 1959), Part 1.
[36] For a single component film, the grand canonical surface free energy $\psi = -\phi A$, and thus minimizing ψ is equivalent to maximizing ϕ.